Research Square

Preprints are preliminary reports that have not undergone peer review.
They should not be considered conclusive, used to inform clinical practice,
or referenced by the media as validated information.

DSCAM and COL4A2 contribute to neuronal and astrocytic spatial organization during brain development

Kento Hizawa
Tohoku University
Tatsuya Ikuta
Keio University School of Medicine
Tomoki Nishioka
Fujita Health University
Natsumi Honjoya
Tohoku University
Yukiko U. Inoue
National Center of Neurology and Psychiatry
Takayoshi Inoue
National Center of Neurology and Psychiatry
Kozo Kaibuchi
Fujita Health University
Mikio Hoshino
National Center of Neurology and Psychiatry
Takuya Sasaki
Tohoku University
Nariko Arimura
nariko.arimura.a2@tohoku.ac.jp
Tohoku University

Research Article

Keywords: DSCAM, COL4A2, cellular distribution, astrocyte, cortical organization

Posted Date: November 25th, 2026

DOI: https://doi.org/10.21203/rs.3.rs-11849038/v1

License: This work is licensed under a Creative Commons Attribution 4.0 International License.
Read Full License

Additional Declarations: No competing interests reported.

DSCAM and COL4A2 contribute to neuronal and astrocytic spatial organization during brain development

Kento Hizawa[a], Tatsuya Ikuta[b], Tomoki Nishioka[c], Natsumi Honjoya[a], Yukiko U. Inoue[d], Takayoshi Inoue[d], Kozo Kaibuchi[c], Mikio Hoshino[d], Takuya Sasaki [a, e], Nariko Arimura [a]

Affiliations

[a] Department of Pharmacology, Graduate School of Pharmaceutical Sciences, Tohoku University, 6-3, Aoba, Aramaki, Aoba-ku, Sendai, Miyagi 980-8578, Japan

[b] The Sakaguchi Laboratory, Department of Signal Exploration, Keio University School of Medicine, 35 Shinanomachi, Shinjuku-ku, Tokyo 160-8582, Japan

[c] Division of Molecular Cell Biology, International Center for Brain Science, Fujita Health University, 1-98 Dengakugakubo, Kutsukake-cho, Toyoake, Aichi 470-1192, Japan

[d] Department of Biochemistry and Cellular Biology, National Institute of Neuroscience, National Center of Neurology and Psychiatry, 4-1-1 Ogawa-higashi, Kodaira, Tokyo 187-8502, Japan

[e] Department of Neuropharmacology, Graduate School of Medicine, Tohoku University, 2-1 Seiryo-machi, Aoba-ku, Sendai, Miyagi 980-8575, Japan

Corresponding author: Nariko Arimura (nariko.arimura.a2@tohoku.ac.jp)

ORCID: https://orcid.org/0000-0001-8998-260X

Acknowledgements

We thank Ms. Yukari Nikami and Ms. Eiko Fukuda for their technical assistance. The figures were created using BioRender.com.

Number of Pages: 44

Number of Figures: 5

Number of tables: 0

Number of Supplementary Tables: 2

Abstract

Down syndrome cell adhesion molecule (DSCAM) is a neuronal cell adhesion molecule implicated in the regulation of neuronal tiling, synaptic specificity, and neuronal spacing during brain development. Although DSCAM regulates neuronal tiling and selective cell–cell interactions, whether it cooperates with extracellular matrix proteins to establish cortical cellular distribution remains unknown. Here, we identified type IV collagen α2 (COL4A2), a major component of the vascular basement membrane, as a novel DSCAM-associated protein using immunoprecipitation coupled with liquid chromatography–tandem mass spectrometry, followed by reciprocal co-immunoprecipitation analysis. Structural predictions using AlphaFold3 suggested a potential interaction between the extracellular domains of DSCAM and COL4A2. Knockdown of *Dscam* increased cell–cell contact without significantly altering the mean distance between neighboring cells in a three-dimensional type I collagen culture system. Furthermore, in utero knockdown of either *Dscam* or *Col4a2* using antisense oligonucleotides (ASOs) altered the regional distribution of GFAP-positive cells in the developing cerebral cortex. These findings identify COL4A2 as a novel DSCAM-associated extracellular protein and suggest that DSCAM- and COL4A2-dependent mechanisms contribute to cortical cellular distribution during brain development.

Keywords

DSCAM; COL4A2; cellular distribution; astrocyte; cortical organization

Introduction

The mature mammalian brain comprises neurons and glial cells that cooperate to establish functional neural circuits. Neurons in the neocortex are organized into six distinct cortical layers, a characteristic cytoarchitecture that underlies higher brain functions (Brodmann 1909; Brodmann 1910; Harris and Shepherd 2015). This highly ordered cellular architecture is progressively established during embryonic and early postnatal development through coordinated neuronal migration, neurite extension, and interactions between neurons and glial cells (Lago-Baldaia et al. 2020; Rakic 2007; Takahashi et al. 1999). Immature neurons undergo dynamic changes in cell–cell adhesion as they migrate and establish their positions within the developing cerebral cortex during embryonic development (Sekine et al. 2011). Following birth, astrocytes rapidly proliferate and progressively migrate into the spaces between neurons, establishing their positions within developing neural circuits (Bushong et al. 2002; Clarke and Barres 2013; Ge et al. 2012). However, the molecular mechanisms underlying the highly ordered cellular architecture are poorly understood.

Astrocytes are a major glial cell population in the central nervous system and play an indispensable role in neural circuit formation and maturation (Allen and Lyons 2018; Sofroniew and Vinters 2010). They regulate synapse formation and elimination, extracellular ion homeostasis, metabolic support, and establishment and maintenance of the blood–brain barrier (Abbott et al. 2006; Chung et al. 2015; Sofroniew and Vinters 2010). Recent lineage-tracing studies have demonstrated that astrocyte precursors are regionally specified before migration and subsequently establish characteristic spatial distributions within the central nervous system (Hochstim et al. 2008; Tsai et al. 2012). During early postnatal development, astrocytes rapidly elaborate their processes and form non-overlapping territorial domains among neighboring neurons (Bushong et al. 2004). These findings suggest that the precise spatial relationship between neurons and astrocytes is critical for normal circuit development (Halassa et al. 2007). Nevertheless, the molecular mechanisms that coordinate neuronal-astrocyte

distribution remain largely unknown.

Down syndrome cell adhesion molecule (DSCAM) is a transmembrane cell adhesion molecule belonging to the immunoglobulin superfamily (Schmucker et al. 2000; Yamakawa et al. 1998). The extracellular region of DSCAM consists of multiple immunoglobulin and fibronectin type III domains, followed by a single transmembrane domain and a cytoplasmic tail (Yamakawa et al. 1998). DSCAM has been implicated in both adhesive and repulsive cell–cell interactions. DSCAM contributes to selective synapse formation via adhesive interactions (Yamagata and Sanes 2008). In contrast, DSCAM mediates dendritic self-avoidance and regulates neuronal cell body spacing, thereby contributing to proper spatial organization of neurons (Fuerst et al. 2009; Fuerst et al. 2008; Yamagata and Sanes 2008). In *Dscam* mutant mice, retinal neurons exhibit abnormal clustering and dendritic fasciculation, indicating that DSCAM is essential for proper neuronal spacing and tissue organization (Fuerst et al. 2009; Fuerst et al. 2008). We previously demonstrated that DSCAM regulates neuronal delamination through the RapGEF2–Rap1–N-cadherin signaling pathway and that *Dscam* knockdown in the embryonic mouse brain induces ectopic neuronal aggregation (Arimura et al. 2020). Furthermore, naturally occurring *Dscam* mutant mice exhibit abnormal posture and impaired motor function, and human genetic studies have identified DSCAM as a risk factor for autism spectrum disorder (Satterstrom et al. 2020; Thiry et al. 2018; Xu et al. 2011). Collectively, these findings indicated that DSCAM is a key regulator of neuronal distribution during brain development.

Recent studies have highlighted the importance of extracellular matrix (ECM) proteins in regulating cell migration, adhesion, and tissue architecture during neural development (Long and Huttner 2019; Mubuchi et al. 2024). Fibronectin, for example, interacts with integrin α5β1 to regulate neuronal migration in the developing cerebral cortex (Marchetti et al. 2010; Sekine et al. 2012). However, the extracellular proteins associated with DSCAM and their potential contribution to cortical cellular

106 organization remain poorly understood (Long and Huttner 2019). Therefore, identifying DSCAM-
107 associated extracellular proteins may provide important insights into the molecular mechanisms
108 underlying cortical tissue organization.
109
110 In this study, we identified collagen type IV α2 (COL4A2) as a novel DSCAM-associated extracellular
111 protein. We further investigated the roles of DSCAM and COL4A2 in cellular organization using
112 three-dimensional collagen culture and in utero knockdown approaches. Our findings suggest that
113 DSCAM- and COL4A2-dependent mechanisms contribute to the cortical cellular organization during
114 brain development.

Methods

Animals

Homozygous *Dscam*-3×ALFA knock-in mice (hereafter referred to as *Dscam*$^{ALFA/ALFA}$) (Dewa et al. 2024) and their wild-type littermates were used in this study. Timed-pregnant ICR mice were purchased from Japan SLC, Inc. (Shizuoka, Japan) on embryonic day (E) 11 or E12. The mice were maintained under standard laboratory conditions with controlled temperature and humidity under a 12-h light/12-h dark cycle and had ad libitum access to food and water. Both male and female mice were included in the study, and animals were not selected based on sex. Pregnant mice were anesthetized with a mixture of medetomidine hydrochloride (Domitor, 0.3 mg/kg; Nippon Zenyaku Kogyo, Fukushima, Japan), midazolam (Dormicum, 4 mg/kg; Maruishi Pharmaceutical, Osaka, Japan), and butorphanol tartrate (Vetorphale, 5 mg/kg; Meiji Animal Health Co., Ltd., Kumamoto, Japan) during the surgical procedures to minimize pain and distress.

At the end of the experiment, the mice were deeply anesthetized with 2% isoflurane and euthanized by transcardial perfusion or cervical dislocation. All animal procedures were approved by the Institutional Animal Care and Use Committee of Tohoku University (Approval No. 2024PhA-005) and were performed in accordance with the Guidelines for Animal Experimentation of Tohoku University.

DNA constructs

shRNA-expressing vectors were constructed using previously reported targeting sequences: sh-*Dscam* (5′-GTACATGGACTTGCTGACGTCT-3′) (Yamagata and Sanes 2008) and a control scramble sequence (5′-AATGCATCTCTGCAAGAGGTA-3′) (Purohit et al. 2012). These targeting sequences and their complementary sequences were inserted into the mU6pro vector as previously described, and the knockdown efficiency of sh-*Dscam* was validated (Arimura et al. 2020).

Immunoprecipitation assay

To confirm the expression of DSCAM-3×ALFA, whole brains from postnatal day 10 (P10) wild-type (WT) and *Dscam*$^{ALFA/ALFA}$ mice were homogenized in RIPA buffer, sonicated on ice for 15 sec, and centrifuged at 200,000 × *g* for 10 min at 4 °C. The pellet was resuspended in buffer B from the ULTRARIPA Kit for Lipid Rafts (Funakoshi, Tokyo, Japan). Rabbit anti-ALFA antibody (1 μg; N1581, NanoTag Biotechnologies, Göttingen, Germany) or normal rabbit IgG (1 μg; PM035; MBL, Tokyo, Japan) was added to each sample and incubated for 2 h at 4 °C. Immune complexes were precipitated using a Dynabeads Protein G Immunoprecipitation Kit (Thermo Fisher Scientific, Waltham, MA, USA) according to the manufacturer's instructions.

To identify DSCAM-associated proteins, whole brains were collected from embryonic mice at E15 (*Dscam*$^{+/+}$ and *Dscam*$^{ALFA/ALFA}$; one mouse per genotype at E15). Brain tissues were homogenized in Buffer A of the ULTRARIPA Kit for Lipid Rafts, supplemented with a protease inhibitor cocktail (cOmplete, Roche, Basel, Switzerland), sonicated for 15 sec, and centrifuged at 9,060 × *g* for 10 min. The supernatants were incubated with rabbit anti-ALFA antibody (1 μg) or rabbit IgG (1 μg) for 1 h at 4 °C, followed by incubation with Dynabeads Protein A (Thermo Fisher Scientific) for an additional 1 h. Immunoprecipitated proteins were subjected to silver staining using the 2D Silver Staining Reagent II kit (Cosmo Bio, Tokyo, Japan) or analyzed by liquid chromatography–tandem mass spectrometry (LC–MS/MS) using an Orbitrap Fusion mass spectrometer (Thermo Fisher Scientific).

To confirm the association between DSCAM and collagen IV, reciprocal co-immunoprecipitation assays were performed on the whole brains of postnatal day 3 (P3) mice. Brain tissue was processed as described above. The samples were incubated with rabbit anti-DSCAM antibody (1 μg; HPA019324; Sigma-Aldrich, St. Louis, MO, USA), mouse anti-collagen IV monoclonal antibody (1 μg; clone 1042, 14-9871-82; eBioscience, Thermo Fisher Scientific), or the corresponding control IgG (normal rabbit IgG [1 μg; PM035; MBL, Tokyo, Japan] or mouse IgG isotype control [1 μg; M075-3; MBL]) for 1 h at 4 °C, followed by incubation with Dynabeads Protein A (Thermo Fisher Scientific)

for an additional 1 h. Immunoprecipitated proteins were mixed with 3× sodium dodecyl sulfate (SDS) sample buffer and heated at 95 °C for 5 min. Proteins were separated on 4–20% SDS-polyacrylamide gels and transferred onto polyvinylidene fluoride (PVDF) membranes. The membranes were blocked with 5% skim milk in Tris-buffered saline with Tween-20 (TBST) for 1 h at room temperature and incubated overnight at 4 °C with rabbit anti-DSCAM (1:1000; HPA019324, Sigma-Aldrich) or mouse anti-collagen IV monoclonal antibody (clone 1042, 14-9871-82; eBioscience, Thermo Fisher Scientific). After washing with TBST, the membranes were incubated with horseradish peroxidase (HRP)-conjugated goat anti-rabbit IgG (1:1000; 31460; Invitrogen, Thermo Fisher Scientific) or HRP-conjugated goat anti-mouse IgG (1:1000; 115-035-003; Jackson ImmunoResearch Laboratories, West Grove, PA, USA) for 1 h at room temperature. Immunoreactive bands were detected using Immobilon Forte Western HRP Substrate (Millipore, Burlington, MA, USA) and visualized using an iBright CL750 imaging system (Invitrogen).

LC–MS/MS data analysis

MS/MS spectra were searched against the Mus musculus UniProtKB database using MaxQuant (version 2.0.3.0). Trypsin was specified as the proteolytic enzyme, allowing for up to one missed cleavage step. A target–decoy approach was used to control the false discovery rate with a threshold of 1% at both the peptide and protein levels. Proteins specifically detected in *Dscam*$^{ALFA/ALFA}$ immunoprecipitates, but not in the WT or IgG controls, were considered candidate DSCAM-associated proteins.

Structural prediction of the DSCAM–COL4A2 complex using AlphaFold3

The amino acid sequences of mouse DSCAM and COL4A2 were retrieved from the DDBJ and submitted to the AlphaFold Server using default parameters for structure prediction (Abramson et al. 2024). Full-length DSCAM and COL4A2 were too large for complex prediction, and the selected

regions were analyzed instead, focusing on the FNIII domains (FN3-1 to FN3-6; residues 885–1575) of DSCAM and residues 1481–1707 of COL4A2. The predicted structures were examined using PyMOL, and the model retained in the PyMOL session was used for structural inspection. The confidence of the locally predicted structures was assessed using the predicted local distance difference test (pLDDT) values retained in the model. Predicted aligned error information was not available in the analyzed session and was therefore not included in the present evaluation.

Three-dimensional collagen culture of embryonic neural cells

Low-concentration collagen gel (0.75 mg/mL) was prepared by diluting Cellmatrix Type I-A collagen (3.0 mg/mL; Nitta Gelatin, Osaka, Japan) with dilute hydrochloric acid and mixing it with 10× MEM and collagen gel reconstitution buffer (8:1:1, v/v/v) according to the manufacturer's instructions. Dorsal midbrain tissues were isolated from E15.5 mouse embryos after removing the meninges and dissociated using neuron dissociation solution S (FUJIFILM Wako Pure Chemical Corporation, Osaka, Japan). Approximately 2×10^6 dissociated cells were resuspended in Neurobasal medium (Gibco, Thermo Fisher Scientific) supplemented with 10% fetal bovine serum (FBS). Plasmids were introduced by electroporation using the Neon NxT Electroporation System (Thermo Fisher Scientific) with a custom electroporation program (voltage: 1400 V, pulse width: 20 ms, three pulses). The plasmids used were pCAG-EGFP (2.5 μg/μL), pmU6-Scramble (3.3 μg/μL), and pmU6-sh*Dscam* (2.7 μg/μL). pCAG-EGFP and either pmU6-Scramble or pmU6-sh*Dscam* were mixed at a mass ratio of 1:3. Following electroporation (4.0 μg), the cells were mixed with the collagen solution, seeded onto coverslips placed in 24-well culture plates, and allowed to polymerize at 37 °C for 30 min. Neurobasal medium containing 10% FBS was added, and after 2 h, the medium was replaced with Neurobasal medium supplemented with B27 (Gibco) and GlutaMAX (Gibco). Cultures were maintained at 37 °C in a humidified atmosphere containing 5% CO_2, and the medium was changed every 2 days.

Antisense oligonucleotide (ASO) design

Three antisense oligonucleotide (ASO) formulations were used in this study: control ASO (Ctl ASO), *Dscam*-targeting ASO, and *Col4a2*-targeting ASO. All ASOs were synthesized by Integrated DNA Technologies (IDT, Coralville, IA, USA). *Dscam* and *Col4a2* ASOs were designed as gapmer oligonucleotides, and each formulation consisted of a mixture of four oligonucleotides targeting the respective mRNAs. ASOs contained phosphorothioate (PS) backbone modifications and 2′-O-methoxyethyl (2′-MOE) sugar modifications. The complete ASO sequences and chemical modifications are provided in Online Resource 1.

In utero ASO injection

Timed-pregnant mice at E13.5 were anesthetized by intraperitoneal injection of a mixture of medetomidine hydrochloride (0.3 mg/kg), midazolam (4 mg/kg), and butorphanol tartrate (5 mg/kg), as described above. Following midline laparotomy, the uterine horns were gently exposed and kept moist using sterile phosphate-buffered saline (PBS) throughout the procedure. For single-gene knockdown, four ASOs targeting either *Dscam* or *Col4a2* were mixed at a final concentration of 0.10 mg/mL each, resulting in a total ASO concentration of 0.40 mg/mL. For double knockdown, the four *Dscam*-targeting and four *Col4a2*-targeting ASOs were combined at 0.10 mg/mL each, resulting in a total ASO concentration of 0.80 mg/mL. Ctl ASO was used at 0.40 mg/mL. A total of 2.5 μL of ASO solution was injected into the lateral ventricle of each embryo using an electric microinjector (BJ-120; BEX Co., Ltd., Tokyo, Japan). To minimize litter-to-litter variation, a within-litter experimental design was adopted, in which embryos in one uterine horn received the Ctl ASO, whereas embryos in the contralateral horn received the *Dscam* ASO, *Col4a2* ASO, or a mixture of both ASOs (double knockdown). After injection, the uterus was returned to the abdominal cavity, the abdominal wall was sutured, and pregnant mice were allowed to recover on a heating pad.

Preparation of brain lysates and Western blotting

The forebrains were dissected from embryos (E15.5) or postnatal day 6 (P6) mice treated with ASOs and homogenized in ice-cold homogenization buffer containing 100 mM sucrose, 20 mM Tris-HCl (pH 7.4), 1 mM EDTA, 1 mM DTT, 150 mM NaCl, and a protease inhibitor cocktail (cOmplete, Roche). After centrifugation at 20,000 × *g* for 10 min at 4 °C, the pellet was resuspended in RIPA buffer (10 mM Tris-HCl, pH 7.4, 1 mM EDTA, 150 mM NaCl, and 1% NP-40), supplemented with a protease inhibitor cocktail, and sonicated on ice for 15 sec. Samples were mixed with 3× SDS sample buffer and heated at 95 °C for 5 min. Equal amounts of protein were separated on 4–20% sodium dodecyl sulfate-polyacrylamide gels and transferred onto PVDF membranes. The membranes were blocked with 5% skim milk in TBST for 1 h at room temperature and incubated overnight at 4 °C with rabbit anti-DSCAM (1:1000; HPA019324; Sigma-Aldrich), mouse anti-collagen IV monoclonal antibody (clone 1042; 14-9871-82; eBioscience, Thermo Fisher Scientific), or rabbit anti-β-actin monoclonal antibody (clone 13E5; 1:1000; 4970T; Cell Signaling Technology). After washing with TBST, the membranes were incubated with horseradish peroxidase-conjugated goat anti-rabbit IgG (1:1000; 31460; Invitrogen) or horseradish peroxidase-conjugated goat anti-mouse IgG (1:1000; 115-035-003; Jackson ImmunoResearch Laboratories) for 1 h at room temperature. Immunoreactive bands were detected using Immobilon Forte Western HRP Substrate (Millipore) and visualized using an iBright CL750 imaging system (Invitrogen).

Immunostaining and immunohistochemistry

Cultured cells were fixed with 4% paraformaldehyde (PFA; 400 μL/well) for 10 min at room temperature, permeabilized with 0.3% Triton X-100 on ice for 10 min, and blocked with 10% normal donkey serum (NDS) for 1 h at room temperature. The cells were then incubated with DAPI diluted in blocking solution (1:10,000, 300 μL/well) for 2 h at room temperature, washed three times with PBS for 5 min each, transferred onto glass slides, surrounded with circular spacers, and mounted with

PermaFluor (Epredia, Portsmouth, NH, USA). The EGFP fluorescence was observed directly without antibody staining.

Following euthanasia by cervical dislocation, brains were removed and immersion-fixed overnight in 4% PFA, cryoprotected overnight in 30% sucrose, embedded in O.C.T. compound (Sakura Finetek, Tokyo, Japan), and sectioned coronally at 40 μm using a cryostat (CM3050 S; Leica, Wetzlar, Germany). Sections of the cerebral cortex were mounted on glass slides, immersed in PBS for 10 min, and blocked with PBS containing 10% NDS and 0.3% Triton X-100 for 1 h at room temperature. The sections were then incubated overnight at 4 °C with rabbit anti-GFAP (1:1000; 12389T; Cell Signaling Technology, Danvers, MA, USA) diluted in blocking solution. After washing twice with PBS for 5 min each, the sections were incubated for 2 h at room temperature with NeuroTrace 640/660 Deep-Red Fluorescent Nissl Stain (1:1000; N21483; Thermo Fisher Scientific), Alexa Fluor 594-conjugated AffiniPure F(ab')$_2$ fragment (1:1000; Jackson ImmunoResearch Laboratories), and DAPI (1:10,000) diluted in blocking solution. Finally, the sections were washed twice with PBS for 5 min each and mounted with PermaFluor.

Image acquisition

For each animal, three coronal brain sections at comparable rostrocaudal levels were selected based on the morphology of the hippocampus and the surrounding anatomical landmarks. Images of the upper, middle, and lower cortical regions of each section were acquired. Immunofluorescence images of cultured cells and brain sections were acquired using a ZEISS LSM 980 laser-scanning confocal microscope (Carl Zeiss, Oberkochen, Germany) with a 20× objective. Z-stack images were acquired at 1-μm intervals. Images were acquired under identical settings in each experiment, and the laser power and detector gain were set to avoid pixel saturation during quantitative fluorescence analysis. For three-dimensional neuronal cultures, approximately 90–100 images were acquired along the z-axis across the full thickness of each sample. Z-stack images were reconstructed using the Imaris software

(Oxford Instruments, Abingdon, UK).

Functional enrichment and protein–protein interaction analyses

Proteins identified by LC–MS/MS were subjected to functional enrichment and protein–protein interaction (PPI) network analyses using Metascape (Zhou et al. 2019). Analyses were performed using default settings, including a minimum overlap of 3, a *P*-value cutoff of 0.05, and a minimum enrichment factor of 1.5. Enriched biological terms were visualized as an enrichment network, and protein-interaction relationships were displayed as a PPI network.

Quantification and statistical analysis

Intercellular distances and cell–neurite contacts were quantified from three-dimensionally reconstructed images using Imaris (Oxford Instruments). Based on the observed distribution of intercellular distances, cells located within a 10 μm radius were defined as neighboring cells and included in the analysis. In contrast, cells located more than 10 μm away were excluded. Cells in contact with the neuronal processes were defined as DAPI-positive cells in direct contact with the reconstructed neurites.

For quantitative analysis of the brain sections, three anatomically matched coronal sections containing the hippocampus were analyzed per animal. In each section, the cortical region overlying the hippocampus was divided into upper, middle, and lower regions along the pial-to-hippocampal axis, with the lower region, including the corpus callosum, immediately dorsal to the hippocampus. Values obtained from the three sections were averaged for each region to generate a single value for each animal. GFAP-positive cells with DAPI-positive nuclei were counted manually. Brain weight was measured as the wet weight. For NeuroTrace fluorescence analysis, pixel intensities were measured using Fiji (Schindelin et al. 2012). To compare the relative distribution of fluorescence intensities across images, pixel intensities were normalized to the maximum intensity within each

image and expressed on a scale of 0 to 1. Cumulative distribution functions (CDFs) were generated from normalized intensity values using an approach based on cumulative threshold spectral analysis (Johnson and Walker 2015). Each CDF represents the cumulative proportion of pixels with intensities at or below a given normalized intensity value. Based on an exploratory inspection of the cumulative fluorescence intensity distributions, the normalized intensity range of 0–0.1 was selected to characterize the low-intensity component. The proportion of pixels within this range was calculated for each sample and used for statistical comparisons between the experimental groups. Statistical analyses were performed using GraphPad Prism 10 (GraphPad Software, Boston, MA, USA), whereas NeuroTrace fluorescence intensity distribution analysis and exact permutation tests were performed using Python. No samples were excluded from the analyses unless a technical failure precluded reliable quantification. Differences between the two groups were analyzed using the two-tailed Mann–Whitney *U* test, except for the NeuroTrace fluorescence intensity analysis, for which a two-sided exact permutation test was performed. For the permutation test, the proportion of pixels with normalized fluorescence intensities at or below 0.1 [F (0.1)] was calculated for each animal. The difference in group means (knockdown minus control) was used as the test statistic. All possible reallocations of individual animal values between the groups were enumerated (70 permutations for comparisons of four versus four animals, and 126 permutations for comparisons of four versus five animals). The exact two-sided *P*-value was calculated as the proportion of permutations yielding an absolute difference in group means equal to or greater than the observed absolute difference. $P < 0.05$ was considered statistically significant.

Results

Identification of DSCAM-associated proteins

To identify the proteins associated with DSCAM, we performed immunoprecipitation followed by LC–MS/MS using embryonic brains from *Dscam*$^{ALFA/ALFA}$ knock-in mice and their WT littermates (Fig. 1a). The *Dscam*^{ALFA} mouse line, in which a 3×ALFA tag is inserted into the extracellular domain of DSCAM, has been described previously (Dewa et al. 2024). Immunoprecipitation with an anti-ALFA antibody specifically isolated DSCAM from *Dscam*$^{ALFA/ALFA}$ brains, but not from WT controls. LC–MS/MS analysis identified 397 candidate DSCAM-associated proteins (Online Resource 2).

Functional enrichment and protein–protein interaction (PPI) network analyses of the proteins identified using LC–MS/MS were performed using Metascape (Zhou et al. 2019) (Fig. 1b). Several functional clusters were identified, including RNA processing, cell cycle regulation, Wnt signaling, and ECM-related proteins. Among these, the ECM cluster contained several collagen family members, including COL4A2, COL18A1, COL1A1, and COL6A1, as well as fibronectin (FN1) (Fig. 1c). Collagens are major structural components of the ECM and constitute the vascular and pial basement membranes of the central nervous system. Among the collagen-related proteins identified using LC–MS/MS, COL4A2 exhibited the highest peptide abundance in DSCAM immunoprecipitates (Fig. 1c). Because type IV collagen is a major component of the brain basement membrane and has been implicated in brain development (Takeuchi et al. 2015; Xu et al. 2019), we selected COL4A2 for further analysis.

To further examine the association between DSCAM and collagen IV, reciprocal co-immunoprecipitation followed by western blotting was performed using lysates prepared from the forebrains of P3 mice (Fig. 1d). Although weak nonspecific signals for collagen IV were detected in the IgG control lanes, collagen IV was specifically detected in the DSCAM immunoprecipitates.

Conversely, DSCAM was detected in the collagen IV immunoprecipitates. These findings support the association between DSCAM and collagen IV in the developing mouse brain.

To further investigate the structural basis of the DSCAM–COL4A2 association, structural prediction was performed using AlphaFold3 (Abramson et al. 2024) (Fig. 1e). Because full-length DSCAM and COL4A2 are large proteins, structural predictions were performed using their extracellular domains. While the N-terminal region of DSCAM (residues 1–884) failed to generate a converged model, the C-terminal region (residues 885–1575) containing the FNIII domains produced a stable structural prediction. The predicted model suggested that the second FNIII domain of DSCAM interacts with the C-terminal region of COL4A2 (residues 1481–1707) through multiple putative amino acid interactions, including hydrophobic contacts and hydrogen bonds (Fig. 1e). These structural predictions were consistent with the possibility of a direct interaction between the extracellular domains of DSCAM and COL4A2.

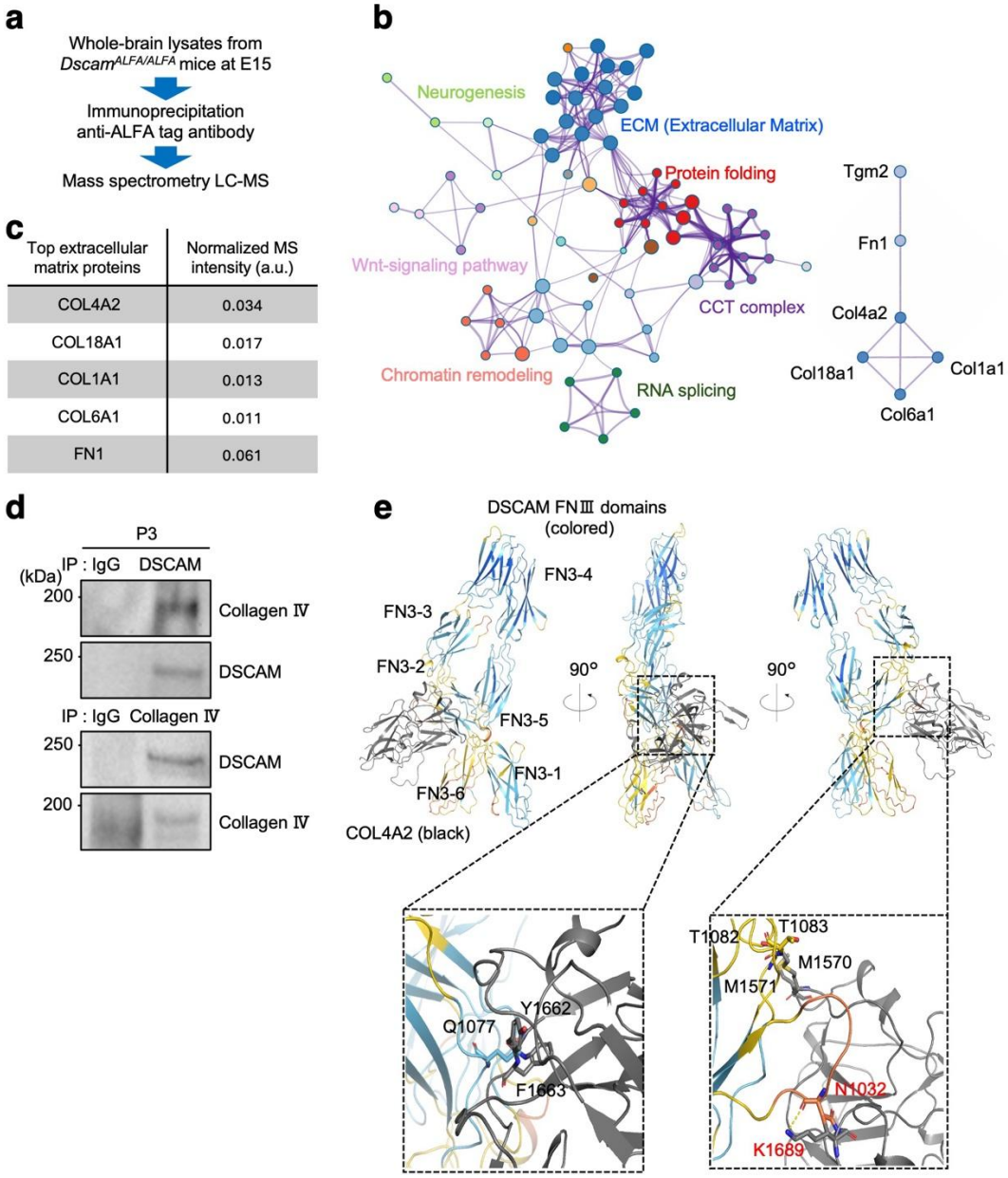

Fig. 1 Proteomic identification of COL4A2 as a DSCAM-associated extracellular matrix protein

(a) Experimental strategy for identifying DSCAM-interacting proteins. Whole-brain lysates from embryonic day (E) 15 *Dscam*$^{ALFA/ALFA}$ mice were subjected to immunoprecipitation using an anti-ALFA antibody, followed by liquid chromatography–tandem mass spectrometry (LC–MS/MS).

(b) Functional enrichment analysis of proteins identified using LC–MS/MS with Metascape. Extracellular matrix (ECM)-related proteins are indicated in blue text and were significantly enriched among DSCAM-associated proteins based on Metascape criteria ($P < 0.05$; enrichment factor > 1.5).

(c) Representative extracellular matrix proteins identified using LC–MS/MS. MS intensities of

candidate proteins were normalized to the MS intensity of DSCAM in the same sample. COL4A2 showed the highest normalized MS intensity among the collagen family proteins detected.
(d) Co-immunoprecipitation analysis demonstrating an association between DSCAM and collagen IV in mouse brains at postnatal day 3 (P3). Immunoprecipitation was performed using anti-DSCAM or anti-collagen IV antibodies, followed by immunoblotting with the indicated antibodies.
(e) Structural prediction of the DSCAM–COL4A2 complex using AlphaFold3. The predicted interaction involves the FNIII domains of DSCAM and the C-terminal region of COL4A2. Enlarged views highlight representative residues predicted to contribute to the interaction interface.

Functional analysis of DSCAM in a three-dimensional collagen culture system

Previous studies primarily examined DSCAM function using conventional two-dimensional neuronal cultures. However, under these conditions, neurites frequently overlap and neuronal aggregation occurs despite endogenous DSCAM expression, making it difficult to evaluate DSCAM-dependent self-avoidance. As our proteomic analysis identified COL4A2 as a novel DSCAM-associated extracellular protein, we hypothesized that extracellular collagen may contribute to DSCAM-dependent neuronal distribution. Therefore, we established a three-dimensional collagen gel culture system and examined the effects of *Dscam* knockdown on neuronal morphology and cell–cell distribution.

For three-dimensional neuronal culture, dissociated cells from the dorsal midbrain of E15.5 mouse embryos were electroporated with either pmU6-Scramble plus pCAG-EGFP (control) or pmU6-sh*Dscam* plus pCAG-EGFP (*Dscam* knockdown; *Dscam* KD) (Arimura et al. 2020). The cells were embedded in a gel composed primarily of type I collagen and cultured for 5 days before fixation and immunostaining (Fig. 2a, b). To evaluate cellular distribution, z-stack confocal images covering the entire thickness of the collagen gel were reconstructed in three dimensions using the Imaris software. Under control conditions, EGFP-positive cells were relatively uniformly distributed

throughout the collagen matrix. In contrast, *Dscam* knockdown resulted in a more clustered distribution of EGFP-positive cells in the three-dimensional collagen gel (Fig. 2c). Quantitative analysis revealed that *Dscam* knockdown significantly increased the proportion of adherent neighboring cells within 10 μm (Fig. 2d, left), whereas the mean distance between neighboring cells within 10 μm was not significantly altered (Fig. 2d, right). These results indicate that the loss of DSCAM promotes cell–cell adhesion without affecting the average spacing between neighboring cells in a three-dimensional collagen environment.

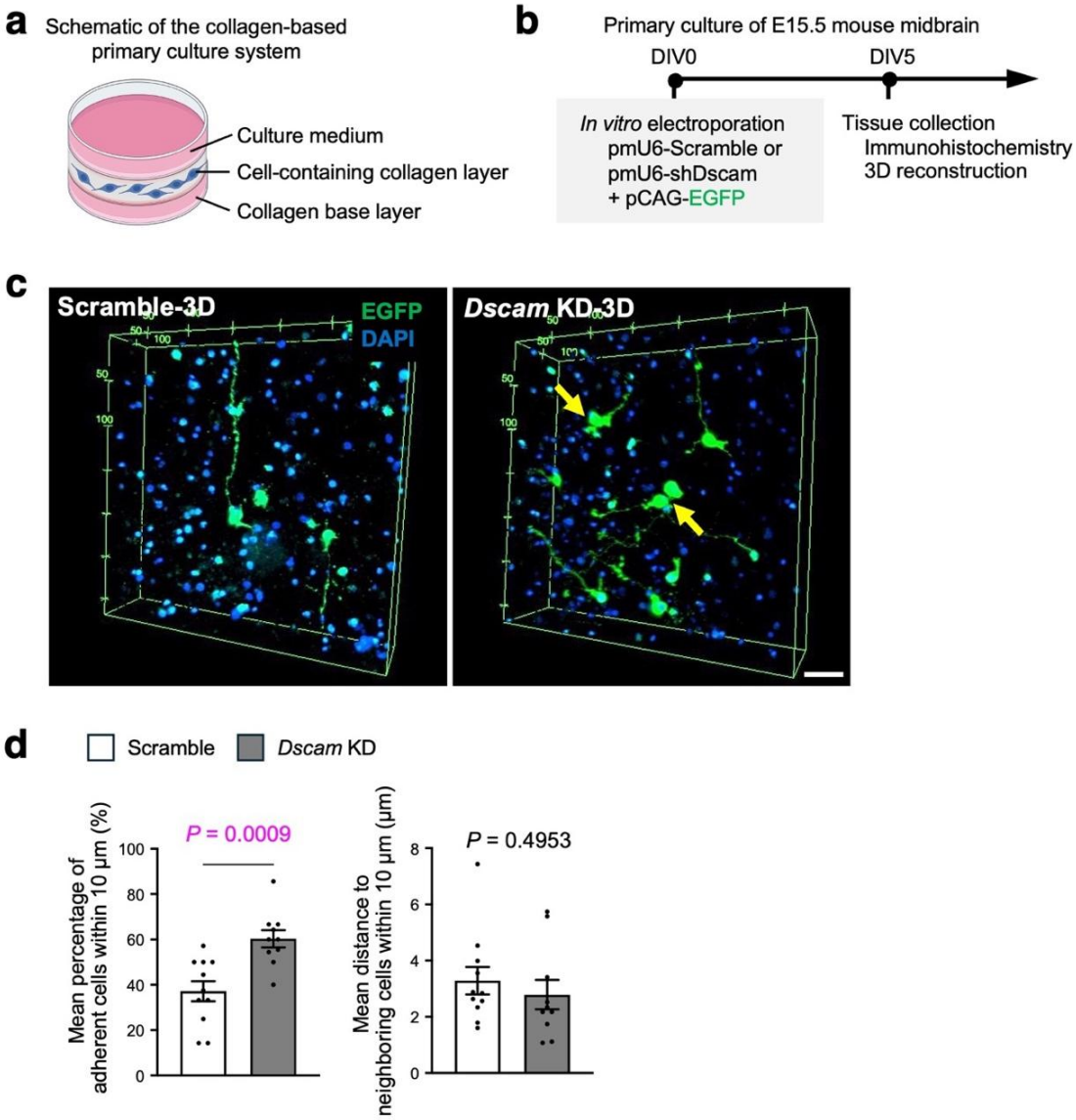

Fig. 2 DSCAM knockdown increases neuronal cell–cell contact in a three-dimensional collagen

matrix

(a) Schematic illustration of the collagen-based three-dimensional (3D) primary culture system. Primary neurons were cultured on a collagen base layer and embedded in a cell-containing collagen gel.

(b) Experimental timeline. Primary midbrain neurons were prepared from embryonic day (E) 15.5 mouse embryos. Neurons were transfected with pmU6-Scramble or pmU6-sh*Dscam* together with pCAG-EGFP by in vitro electroporation at DIV0 and cultured in the collagen matrix for five days before immunostaining and 3D reconstruction.

(c) Representative three-dimensional reconstructions of EGFP-positive neurons cultured in the collagen matrix following transfection with scramble or pmU6-sh*Dscam* together with pCAG-EGFP. EGFP-positive neurons in the *Dscam* knockdown condition exhibited altered neurite morphology and increased cell–cell contact compared with the scramble condition, as indicated by yellow arrows. Scale bar: 50 μm.

(d) Quantification of the percentage of adherent neighboring cells and the mean intercellular distance within a 10-μm range in three-dimensional collagen cultures. *Dscam* knockdown significantly increased the percentage of adherent neighboring cells without significantly altering the mean distance between neighboring cells. Data are presented as mean ± SEM (Scramble, $n = 11$; *Dscam* KD, $n = 10$). For each embryo-derived culture, measurements from multiple cells were averaged, and the resulting mean value was treated as one biological replicate. Statistical significance was determined using the two-tailed Mann–Whitney U test.

Knockdown of *Dscam* and *Col4a2* using antisense oligonucleotides

To investigate the function of COL4A2 during brain development, we first examined the cellular expression pattern of *Col4a2* using a published single-cell RNA sequencing (scRNA-seq) dataset from the E15.5 mouse midbrain (Tiklová et al. 2019). *Col4a2* mRNA was highly enriched in

endothelial cells and pericytes, whereas its expression in neuronal and glial populations was relatively low (Fig. 3a). Based on these findings, we performed in utero intraventricular administration of ASOs. Prenatally administered ASOs are broadly distributed throughout the developing brain (Clarke et al. 2024). The blood–brain barrier is still undergoing functional maturation at E13.5 (Ben-Zvi et al. 2014). Therefore, we expected the intraventricularly administered ASOs to be distributed from the ventricular compartment into the brain parenchyma and reach the vascular cells, thereby suppressing *Dscam* expression in parenchymal neurons, as well as *Col4a2* expression in endothelial cells and pericytes (Fig. 3b, c). To evaluate the knockdown efficiency of the ASOs, western blot analysis was performed using forebrain lysates collected at E15.5 and P6 from mice that received in utero ASO injections at E13.5 (Fig. 3d). Compared to the Ctl ASO group, collagen IV protein levels were reduced in the *Col4a2* ASO group, whereas DSCAM protein levels were reduced in the *Dscam* ASO group at both developmental stages. In contrast, the actin protein levels remained unchanged in both ASO-treated groups (Fig. 3d). The simultaneous administration of *Dscam* and *Col4a2* ASOs reduced both DSCAM and collagen IV immunoreactivity. These findings demonstrate reduced DSCAM and collagen IV signals in forebrain lysates following in utero ASO administration from the embryonic stage through the early postnatal period.

Using the ASO-mediated knockdown strategy described above, we next examined the developmental phenotypes at P6. Since *Dscam* loss-of-function mice exhibit structural abnormalities in the developing brain (Xu et al. 2011), we first assessed whether transient knockdown of *Dscam* and/or *Col4a2* affected overall brain growth by measuring brain weight. Compared to the Ctl ASO group, brain weight was significantly reduced in the *Col4a2* ASO group (Fig. 3e). A similar decrease was observed in the *Dscam* ASO group. Similarly, the simultaneous knockdown of *Dscam* and *Col4a2* resulted in a significant reduction in brain weight (Fig. 3e).

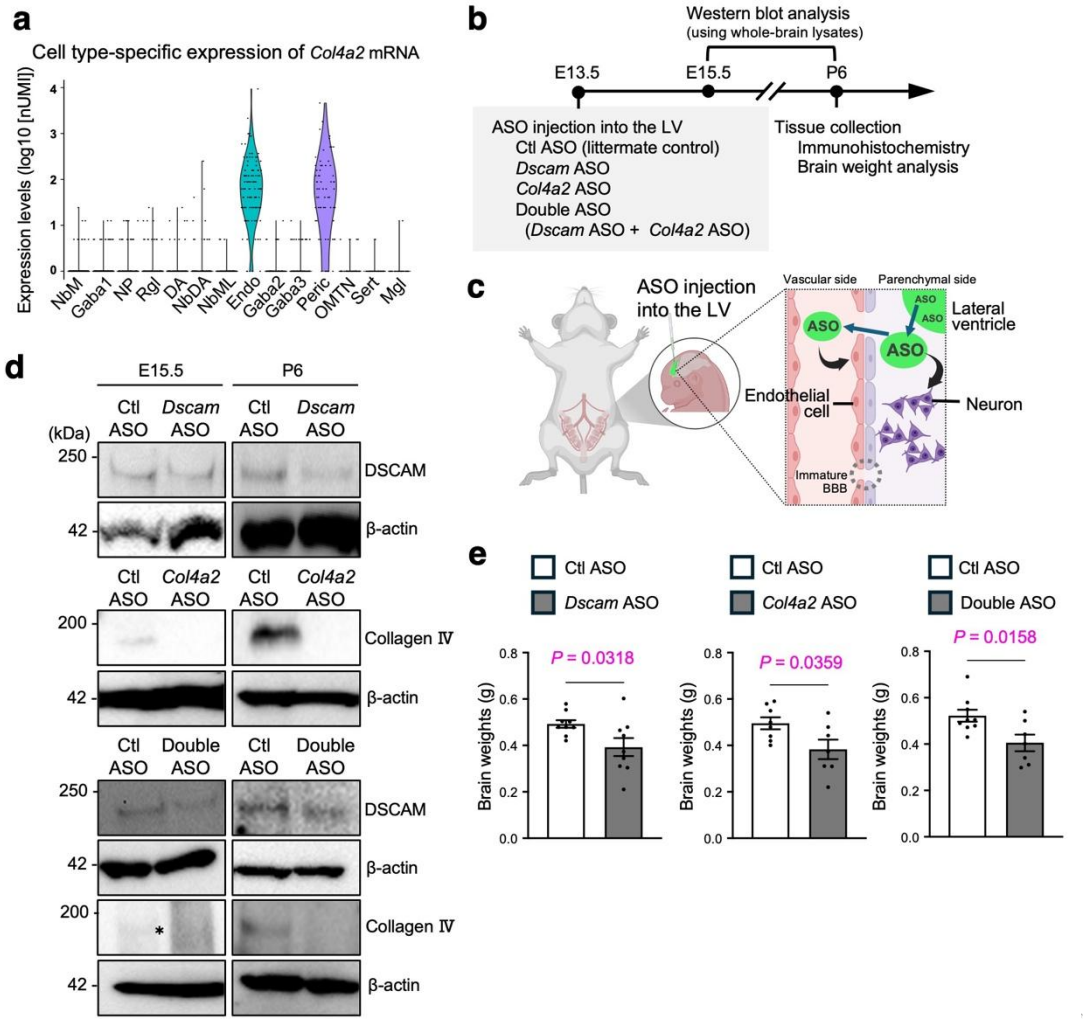

Fig. 3 *Dscam* and *Col4a2* knockdown reduce brain weight

(a) Cell type-specific expression of *Col4a2* mRNA in the developing mouse brain. The plot was generated using the E15.5 mouse midbrain single-cell RNA-sequencing dataset from a published study (Tiklová et al. 2019). *Col4a2* is predominantly expressed in endothelial cells (Endo) and pericytes (Peric). NbM, Medial Neuroblast; Gaba, GABAergic neuron; NP, Neuronal Progenitor; Rgl, Radial glia; DA, Dopaminergic neuron; NbDA, Dopaminergic neuroblast; NbML, Mediolateral Neuroblast; Endo, Endothelial cell; Peric, Pericyte; OMTN, OculoMotor and Trochlear Nucleus; Sert, Serotonergic neuron; Mgl, Microglia; UMI, unique molecular identifier.

(b) Experimental timeline. Control (Ctl), *Dscam*, and/or *Col4a2* ASOs were injected into the lateral ventricle at embryonic day (E) 13.5. Forebrain lysates were collected at E15.5 and postnatal day (P) 6 for western blot analysis, and brains were collected at P6 for immunohistochemistry and brain weight

478 measurements.

479 (c) Schematic illustration of the proposed distribution of ASOs following in utero intraventricular
480 administration. ASOs were expected to distribute into the developing brain parenchyma and potentially
481 reach neural and vascular cells (Borges et al. 2025; Clarke et al. 2024).

482 (d) Western blot analysis showing reduced DSCAM and collagen IV protein levels following ASO
483 administration. Forebrain lysates collected at E15.5 and P6 were immunoblotted with the indicated
484 antibodies. β-actin was used as a loading control.

485 (e) Brain weight measurements following ASO treatment. Brain weight was significantly reduced
486 under all knockdown conditions. Data are presented as mean ± SEM (Ctl ASO, n = 9 from 3 litters;
487 *Dscam* ASO, n = 9 from 3 litters; Ctl ASO, n = 8 from 4 litters; *Col4a2* ASO, n = 7 from 4 litters; Ctl
488 ASO, n = 9 from 3 litters; Double ASO, n = 7 from 3 litters). Statistical significance was determined
489 using the two-tailed Mann–Whitney U test.

490

491 **Effects of Dscam and Col4a2 knockdown on cortical cellular organization**

492 Previous studies have shown that *Dscam* deficiency disrupts neuronal distribution during brain
493 development, resulting in ectopic neuronal aggregation (Arimura et al. 2020; Fuerst et al. 2008). In
494 addition, astrocytes play essential roles in postnatal cortical maturation by infiltrating the neuronal
495 layer and establishing neuron–astrocyte interactions (Bushong et al. 2004; Ge et al. 2012;
496 Lanjakornsiripan et al. 2018). To examine whether the knockdown of *Dscam* and/or *Col4a2* alters
497 the spatial distribution of neurons and astrocytes, we performed double staining with NeuroTrace, a
498 fluorescent Nissl stain, and GFAP, an astrocyte marker (Fig. 4, 5). For all analyses of cellular
499 distribution, littermates were used for comparisons within each experiment (Ctl ASO vs. *Col4a2*
500 ASO, Ctl ASO vs. *Dscam* ASO, and Ctl ASO vs. *Dscam* and *Col4a2* double-KD) to minimize
501 variability in embryonic brain development. The cortical region overlying the hippocampus was
502 divided into the upper, middle, and lower regions, as described above, and each region was analyzed

503 separately (Fig. 4a). To characterize the distribution of NeuroTrace fluorescence intensities
504 quantitatively, the cumulative proportion of pixels below each normalized intensity value was
505 calculated (Fig. 4b). No significant differences in NeuroTrace fluorescence were detected in the
506 upper or lower cortical regions in any of the three knockdown groups compared to their respective
507 littermate controls (Fig. 4c, d, f). In contrast, *Dscam* and *Col4a2* single knockdown significantly
508 increased the proportion of low-intensity NeuroTrace pixels in the middle cortical region, whereas
509 double knockdown showed a similar trend that did not reach statistical significance ($P = 0.0556$)
510 (Fig. 4c, e). Double staining revealed that the GFAP-positive astrocytes (yellow arrows)
511 preferentially accumulated in regions exhibiting reduced NeuroTrace fluorescence within the middle
512 cortical region (Fig. 4c, e). These findings indicate that *Dscam* or *Col4a2* knockdown significantly
513 altered the low-intensity component of NeuroTrace fluorescence in the middle cortical region, with a
514 similar but non-significant trend following double knockdown (Fig. 4g).
515

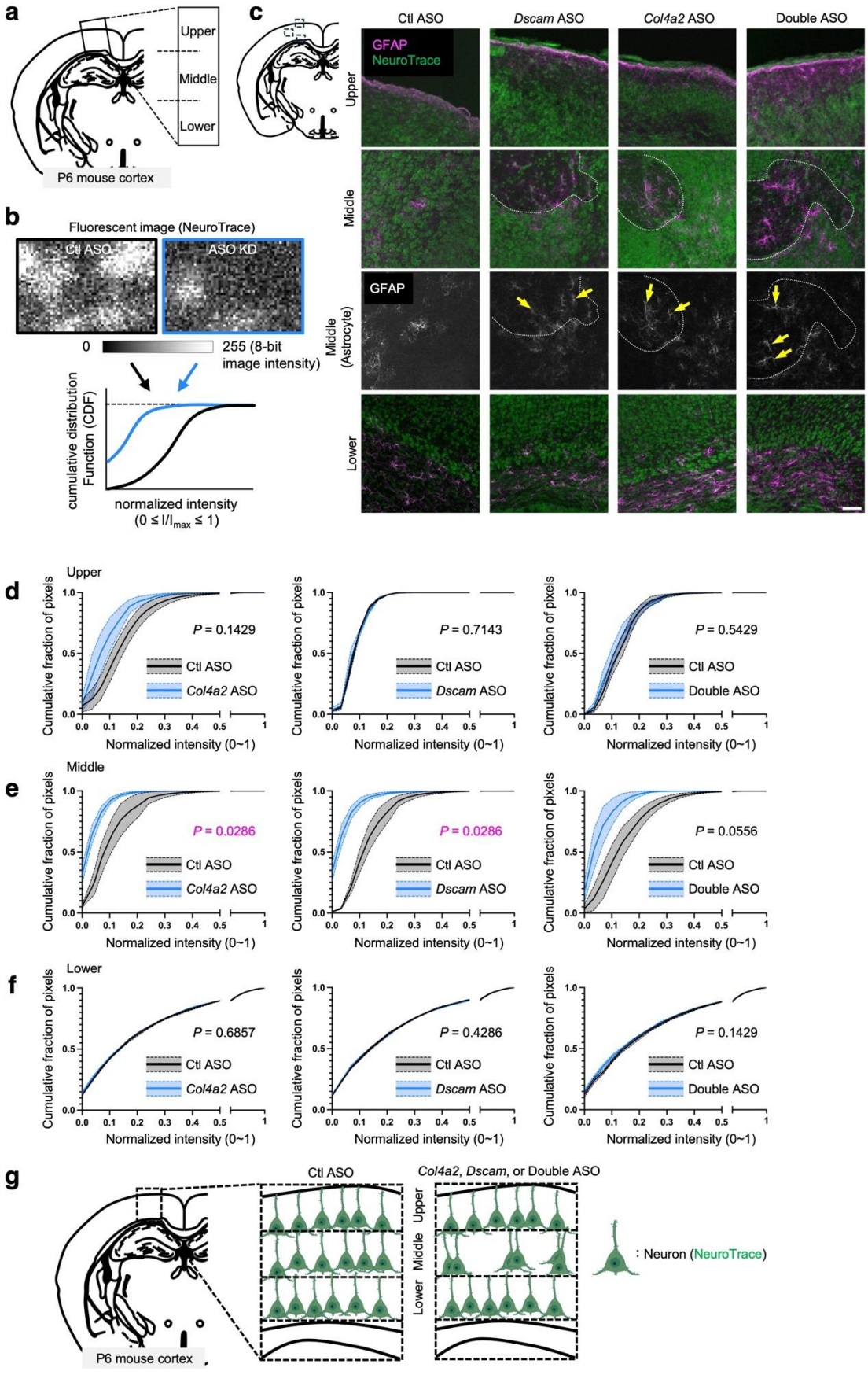

Fig. 4 *Dscam* and *Col4a2* knockdown alter NeuroTrace fluorescence distribution in the

developing cortex

(a) Schematic illustration of the regions of interest (ROIs) used for quantitative analysis of NeuroTrace fluorescence in the P6 mouse cerebral cortex. The cortical region overlying the hippocampus was divided into upper, middle, and lower regions along the pial-to-hippocampal axis. The lower region included the corpus callosum immediately dorsal to the hippocampus. Images were acquired from the center of each region using a 20× objective.

(b) Schematic illustration of the image analysis workflow. NeuroTrace fluorescence intensity within each ROI was measured on a pixel-by-pixel basis, normalized, ranked from low to high intensity, and plotted as cumulative probability distributions.

(c) Representative images of GFAP immunostaining (magenta) and NeuroTrace staining (green) in the upper, middle, and lower cortical regions of P6 mice treated with Control (Ctl), *Dscam*, *Col4a2*, or double (*Dscam* + *Col4a2*) ASOs. GFAP immunostaining in the middle cortical region is additionally shown in grayscale. Scale bar: 30 μm.

(d–f) Cumulative distribution functions (CDFs) of the normalized NeuroTrace fluorescence intensity in the upper (d), middle (e), and lower (f) cortical regions. For each animal, the cumulative proportion of pixels with normalized intensities at or below 0.1 [F (0.1)] was calculated and compared between groups using a two-sided exact permutation test based on the difference in group means. Solid lines indicate the mean CDF, and dashed lines indicate the SEM. ASO-treated littermates were used as controls for each comparison. For the *Dscam* and *Col4a2* ASO comparisons, $n = 4$ per group from 2 litters in all cortical regions. For the double ASO comparison, $n = 4$ per group from 2 litters in the upper and lower regions, whereas $n = 4$ control mice and $n = 5$ double ASO-treated mice were analyzed in the middle region.

(g) Schematic illustration of the changes in cortical NeuroTrace fluorescence patterns following *Dscam* and/or *Col4a2* knockdown. Significant changes were detected in the middle cortical region following a single knockdown, whereas double knockdown showed a similar but non-significant trend

(P = 0.0556). The schematic does not represent direct quantification of neuronal positions or cell numbers.

Effects of Dscam and Col4a2 knockdown on GFAP-positive cell distribution

Next, we examined GFAP-positive astrocyte density in the developing cerebral cortex (Fig. 5a). No significant differences in GFAP-positive astrocyte density were detected across the combined upper, middle, and lower regions in any of the three knockdown groups compared to their respective littermate controls (Fig. 5b–d). However, analysis of individual regions revealed a significant increase in astrocyte density in the middle region following *Dscam* or *Col4a2* knockdown. The simultaneous knockdown of *Dscam* and *Col4a2* significantly increased astrocyte density in both the upper and middle regions (Fig. 5b–d). Together with the altered NeuroTrace fluorescence patterns observed in Fig. 4, these findings suggest that the knockdown of *Dscam* and/or *Col4a2* is associated with alterations in cortical cellular organization (Fig. 5e).

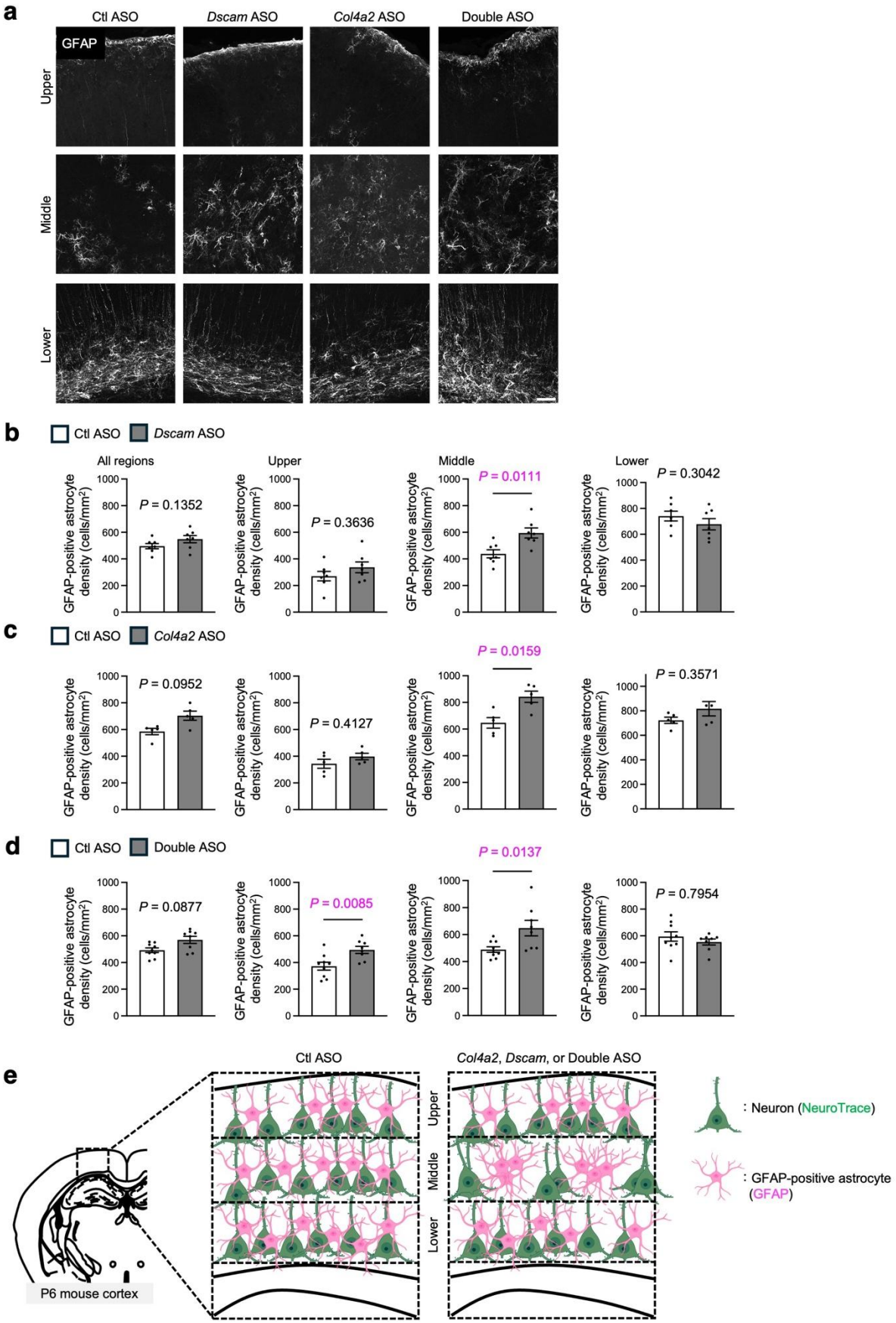

Fig. 5 *Dscam* and *Col4a2* knockdown increase GFAP-positive astrocyte density in specific

cortical regions

(a) Representative images of GFAP-positive immature astrocytes in the upper, middle, and lower cortical regions of P6 mice treated with Control (Ctl), *Dscam*, *Col4a2*, or double ASOs. Scale bar: 30 μm.

(b–d) Quantification of GFAP-positive astrocyte density in mice treated with *Dscam* ASO (b), *Col4a2* ASO (c), or double ASOs (d), each compared with their corresponding Ctl ASO-treated littermates. GFAP-positive astrocyte densities across the combined upper, middle, and lower regions, as well as in each region separately, were quantified. Data are presented as mean ± SEM (Ctl ASO, $n = 7$ from 3 litters; *Dscam* ASO, $n = 7$ from 3 litters; Ctl ASO, $n = 5$ from 2 litters; *Col4a2* ASO, $n = 5$ from 2 litters; Ctl ASO, $n = 9$ from 3 litters; and Double ASO, $n = 8$ from 3 litters). Statistical significance was determined using a two-tailed Mann–Whitney U test. *P*-values are shown in each panel.

(e) Schematic representation of common GFAP-positive astrocyte distribution observed following *Col4a2* ASO, *Dscam* ASO, or combined *Col4a2* + *Dscam* ASO treatment.

Discussion

In the present study, we identified COL4A2 as a novel DSCAM-associated protein by immunoprecipitation, proteomic analysis, and structural prediction using AlphaFold3. Functional analyses using a three-dimensional collagen culture system and in utero ASO-mediated knockdown further demonstrated that suppression of either *Dscam* or *Col4a2* disrupts neuronal and astrocyte distribution during cortical development. Together, these findings identify COL4A2 as a previously unrecognized DSCAM-associated molecule and suggest that interactions between DSCAM and the extracellular matrix contribute to the establishment of a normal cortical cellular distribution.

ECM-dependent DSCAM function

Our biochemical and functional analyses further suggested that the spatial organizing activity of DSCAM was evident in the three-dimensional collagen-containing environment. In conventional two-dimensional neuronal cultures, neurons and their processes are confined to a single plane (LaPlaca et al. 2005), where cell–cell contacts, neurite fasciculation, and cellular aggregation readily occur despite endogenous DSCAM expression (Noble et al. 1984). Under these conditions, it is difficult to evaluate the mechanisms that regulate three-dimensional cellular spacing. In contrast, neurons cultured in the three-dimensional collagen matrix exhibited a relatively uniform distribution, whereas *Dscam* knockdown resulted in prominent neuronal clustering. These findings suggest that the extracellular matrix is not merely a structural scaffold but also provides an environment in which DSCAM can regulate neuronal distribution.

Cooperative regulation of the balance between cell–cell and cell–ECM adhesion by DSCAM and COL4A2

Another major finding of this study was the identification of COL4A2 as a DSCAM-associated extracellular protein. Type IV collagen is a major component of the basement membrane and

599 regulates cell–ECM adhesion through receptors such as integrins (Edwards and Bix 2019; Thomsen
600 et al. 2017). Our biochemical analyses and structural predictions suggest that DSCAM is associated
601 with COL4A2, suggesting that DSCAM functions within a collagen-rich extracellular environment.
602 Although COL4A2 showed the highest peptide abundance among the collagen-related proteins
603 identified in the DSCAM immunoprecipitates, several other extracellular matrix proteins, including
604 FN1 and COL18A1, were also identified as candidate DSCAM-associated molecules. Therefore, it is
605 important to determine whether DSCAM broadly cooperates with extracellular matrix proteins
606 through common molecular mechanisms, potentially involving integrin-mediated cell–ECM
607 adhesion.
608 We previously demonstrated that DSCAM suppresses RapGEF2–Rap1-mediated N-cadherin-
609 dependent cell–cell adhesion during neuronal delamination (Arimura et al. 2020). Based on the
610 present findings, we propose a hypothetical model in which DSCAM-mediated regulation of cell–
611 cell adhesion and collagen IV-associated cell–ECM interactions cooperatively contribute to the
612 maintenance of appropriate cellular distribution. In this model, collagen IV could provide an
613 extracellular scaffold that facilitates cell–ECM interactions, whereas DSCAM may limit excessive
614 N-cadherin-mediated cell–cell adhesion. Balancing these processes may contribute to the
615 establishment of appropriate neuronal spacing during cortical development.
616 Consistent with this possibility, suppression of either *Dscam* or *Col4a2* resulted in remarkably
617 similar phenotypes, including reduced brain weight, altered neuronal distribution, and abnormal
618 astrocyte positioning. These observations suggest that disruption of cell–cell adhesion or cell–ECM
619 interactions ultimately impairs cortical cellular distribution. Furthermore, the absence of a markedly
620 additive phenotype following simultaneous knockdown suggests that DSCAM- and COL4A2-
621 dependent mechanisms may influence overlapping aspects of cortical cellular distribution during
622 development.
623

Association between neuronal disorganization and astrocyte redistribution

One of the notable findings of the present study was that the knockdown of *Dscam* and/or *Col4a2* was associated with region-dependent alterations in GFAP-positive astrocyte density. NeuroTrace analysis revealed altered fluorescence intensity distribution, particularly within the middle cortical region, whereas the upper and lower regions remained largely unaffected. Simultaneously, the GFAP-positive astrocyte density increased in specific cortical regions, particularly in the middle region. Although no significant differences in astrocyte density were observed across the combined regions, regional analysis revealed a significant increase in astrocyte density following the knockdown. Furthermore, our three-dimensional culture analysis, in which only neighboring cells within a 10-μm radius were evaluated, demonstrated that loss of DSCAM increased local cell–cell contact without significantly altering the average distance between neighboring cells. Taken together, these findings suggest that DSCAM- and COL4A2-dependent mechanisms contribute to region-specific cortical cellular organization during development.

Brain weight in ASO-treated mouse brains

The knockdown of either *Dscam* or *Col4a2* reduced brain weight at P6. Although the cortical thickness was not directly measured, this finding is consistent with previous reports describing cortical abnormalities in *Dscam* mutant mice (Maynard and Stein 2012; Xu et al. 2011). Together with the altered cellular distribution observed in the present study, these findings suggest that the disruption of the functional relationship between DSCAM and COL4A2 may impair normal cortical development.

Potential relevance to neurodevelopmental disorders

These findings may also be relevant to human neurodevelopmental disorders. DSCAM is located on the human chromosome 21 and has been implicated in Down syndrome (Liu et al. 2023; Tang et al.

2021; Yamakawa et al. 1998). Genetic studies have identified DSCAM as a susceptibility gene for autism spectrum disorder (Satterstrom et al. 2020). Although the relationship between the present findings and these disorders remains to be established, the altered DSCAM-dependent regulation of cortical cellular organization may provide a framework for future studies investigating disease-associated developmental abnormalities.

Mutations in COL4A2 have also been associated with a broad spectrum of neurological disorders, including cerebrovascular abnormalities, epilepsy, developmental delay, and cognitive impairment (Bakhtiari et al. 2021; Guey and Hervé 2022; Zagaglia et al. 2018). Although these phenotypes have generally been attributed to defects in the vascular basement membrane, the present findings raise the possibility that COL4A2-dependent extracellular matrix alterations may also be associated with changes in cortical cellular organization. Whether the functional relationship between DSCAM and COL4A2 is relevant to these neurological disorders remains unclear.

Limitations

The present study had several limitations. First, the three-dimensional culture experiments were performed using type I rather than type IV collagen. Since type I collagen is widely used as a scaffold for three-dimensional cell culture, and commercially available type IV collagen preparations are not commonly used to form self-supporting three-dimensional gels, we used a type I collagen matrix to examine DSCAM-dependent cellular organization. Notably, our proteomic analysis identified several collagen family members, including COL1A1, COL6A1, and COL18A1, as candidate DSCAM-associated proteins in addition to COL4A2. These findings raise the possibility that DSCAM may associate with multiple collagen types through similar molecular mechanisms and that the type I collagen matrix may reproduce some aspects of the extracellular environment relevant to DSCAM–COL4A2 interactions. However, whether DSCAM directly interacts with these

673 collagens through a common binding mechanism, or exhibits similar properties in a type IV collagen
674 matrix, remains to be determined.
675 Second, although biochemical analyses and AlphaFold3 structural predictions consistently
676 supported the interaction between DSCAM and COL4A2, the present study did not provide direct
677 evidence that the two proteins bind to each other. Additional biophysical analyses such as surface
678 plasmon resonance or mutational analyses of the predicted binding interface are required to
679 determine whether DSCAM interacts directly with COL4A2.
680 Third, the single-cell RNA-sequencing dataset used to assess the cellular expression pattern of
681 *Col4a2* was derived from the E15.5 mouse midbrain rather than from the cerebral cortex. Therefore,
682 regional differences in *Col4a2* expression cannot be excluded, and the dataset does not directly
683 define its expression pattern in the developing cortex.
684 Finally, the present study employed a transient ASO-mediated knockdown rather than cell
685 type-specific genetic manipulation. Consequently, the relative contributions of neurons, endothelial
686 cells, and pericytes to observed phenotypes remain unclear. Future studies using conditional genetic
687 approaches will help clarify the cellular mechanisms underlying DSCAM–COL4A2-mediated
688 regulation of cortical development.
689
690 *Conclusion*
691 In conclusion, the present study identified COL4A2 as a novel DSCAM-associated extracellular
692 protein and demonstrated that DSCAM and COL4A2 regulate cortical cellular distribution during
693 development. Our findings further suggest that the extracellular matrix provides an important
694 microenvironment for DSCAM-dependent regulation of neuronal and astrocyte distribution. These
695 findings provide new insights into the molecular mechanisms underlying cortical development and
696 establish a conceptual framework linking neuronal adhesion molecules with extracellular matrix
697 proteins.
698

References

Abbott NJ, Rönnbäck L, Hansson E (2006) Astrocyte-endothelial interactions at the blood-brain barrier. Nat Rev Neurosci 7:41-53. https://doi.org/10.1038/nrn1824

Abramson J, Adler J, Dunger J, Evans R, Green T, Pritzel A, Ronneberger O, Willmore L, Ballard AJ, Bambrick J, Bodenstein SW, Evans DA, Hung CC, O'Neill M, Reiman D, Tunyasuvunakool K, Wu Z, Žemgulytė A, Arvaniti E, Beattie C, Bertolli O, Bridgland A, Cherepanov A, Congreve M, Cowen-Rivers AI, Cowie A, Figurnov M, Fuchs FB, Gladman H, Jain R, Khan YA, Low CMR, Perlin K, Potapenko A, Savy P, Singh S, Stecula A, Thillaisundaram A, Tong C, Yakneen S, Zhong ED, Zielinski M, Žídek A, Bapst V, Kohli P, Jaderberg M, Hassabis D, Jumper JM (2024) Accurate structure prediction of biomolecular interactions with AlphaFold 3. Nature 630:493-500. https://doi.org/10.1038/s41586-024-07487-w

Allen NJ, Lyons DA (2018) Glia as architects of central nervous system formation and function. Science 362:181-185. https://doi.org/10.1126/science.aat0473

Arimura N, Okada M, Taya S, Dewa KI, Tsuzuki A, Uetake H, Miyashita S, Hashizume K, Shimaoka K, Egusa S, Nishioka T, Yanagawa Y, Yamakawa K, Inoue YU, Inoue T, Kaibuchi K, Hoshino M (2020) DSCAM regulates delamination of neurons in the developing midbrain. Sci Adv 6:eaba1693. https://doi.org/10.1126/sciadv.aba1693

Bakhtiari S, Tafakhori A, Jin SC, Guida BS, Alehabib E, Firouzbadi S, Bilguvar K, Fahey MC, Darvish H, Kruer MC (2021) Recessive COL4A2 Mutation Leads to Intellectual Disability, Epilepsy, and Spastic Cerebral Palsy. Neurol Genet 7:e583. https://doi.org/10.1212/nxg.0000000000000583

Ben-Zvi A, Lacoste B, Kur E, Andreone BJ, Mayshar Y, Yan H, Gu C (2014) Mfsd2a is critical for the formation and function of the blood-brain barrier. Nature 509:507-11. https://doi.org/10.1038/nature13324

Borges B, Brown SM, Chen WJ, Clarke MT, Herzeg A, Park JH, Ross J, Kong L, Denton M, Smith AK, Lum T, Zada FM, Cordero M, Gupta N, Cook SE, Murray H, Matson J, Klein S, Bennett CF,

Krainer AR, MacKenzie TC, Sumner CJ (2025) Intra-amniotic antisense oligonucleotide treatment improves phenotypes in preclinical models of spinal muscular atrophy. Sci Transl Med 17:eadv4656. https://doi.org/10.1126/scitranslmed.adv4656

Brodmann K (1909) Vergleichende Lokalisationslehre der Grosshirnrinde in ihren Prinzipien dargestellt auf Grund des Zellenbaues. Johann Ambrosius Barth, Leipzig

Brodmann K (1910) Feinere Anatomie des Grosshirns. Julius Springer, Berlin

Bushong EA, Martone ME, Ellisman MH (2004) Maturation of astrocyte morphology and the establishment of astrocyte domains during postnatal hippocampal development. Int J Dev Neurosci 22:73-86. https://doi.org/10.1016/j.ijdevneu.2003.12.008

Bushong EA, Martone ME, Jones YZ, Ellisman MH (2002) Protoplasmic astrocytes in CA1 stratum radiatum occupy separate anatomical domains. J Neurosci 22:183-92. https://doi.org/10.1523/jneurosci.22-01-00183.2002

Chung WS, Allen NJ, Eroglu C (2015) Astrocytes Control Synapse Formation, Function, and Elimination. Cold Spring Harb Perspect Biol 7:a020370. https://doi.org/10.1101/cshperspect.a020370

Clarke LE, Barres BA (2013) Emerging roles of astrocytes in neural circuit development. Nat Rev Neurosci 14:311-21. https://doi.org/10.1038/nrn3484

Clarke MT, Remesal L, Lentz L, Tan DJ, Young D, Thapa S, Namuduri SR, Borges B, Kirn G, Valencia J, Lopez ME, Lui JH, Shiow LR, Dindot S, Villeda S, Sanders SJ, MacKenzie TC (2024) Prenatal delivery of a therapeutic antisense oligonucleotide achieves broad biodistribution in the brain and ameliorates Angelman syndrome phenotype in mice. Mol Ther 32:935-951. https://doi.org/10.1016/j.ymthe.2024.02.004

Dewa KI, Arimura N, Kakegawa W, Itoh M, Adachi T, Miyashita S, Inoue YU, Hizawa K, Hori K, Honjoya N, Yagishita H, Taya S, Miyazaki T, Usui C, Tatsumoto S, Tsuzuki A, Uetake H, Sakai K, Yamakawa K, Sasaki T, Nagai J, Kawaguchi Y, Sone M, Inoue T, Go Y, Ichinohe N, Kaibuchi K, Watanabe M, Koizumi S, Yuzaki M, Hoshino M (2024) Neuronal DSCAM regulates the peri-synaptic

749 localization of GLAST in Bergmann glia for functional synapse formation. Nat Commun 15:458.
750 https://doi.org/10.1038/s41467-023-44579-z
751 Edwards DN, Bix GJ (2019) Roles of blood-brain barrier integrins and extracellular matrix in stroke.
752 Am J Physiol Cell Physiol 316:C252-c263. https://doi.org/10.1152/ajpcell.00151.2018
753 Fuerst PG, Bruce F, Tian M, Wei W, Elstrott J, Feller MB, Erskine L, Singer JH, Burgess RW (2009)
754 DSCAM and DSCAML1 function in self-avoidance in multiple cell types in the developing mouse
755 retina. Neuron 64:484-97. https://doi.org/10.1016/j.neuron.2009.09.027
756 Fuerst PG, Koizumi A, Masland RH, Burgess RW (2008) Neurite arborization and mosaic spacing in
757 the mouse retina require DSCAM. Nature 451:470-4. https://doi.org/10.1038/nature06514
758 Ge WP, Miyawaki A, Gage FH, Jan YN, Jan LY (2012) Local generation of glia is a major astrocyte
759 source in postnatal cortex. Nature 484:376-80. https://doi.org/10.1038/nature10959
760 Guey S, Hervé D (2022) Main features of COL4A1-COL4A2 related cerebral microangiopathies.
761 Cereb Circ Cogn Behav 3:100140. https://doi.org/10.1016/j.cccb.2022.100140
762 Halassa MM, Fellin T, Takano H, Dong JH, Haydon PG (2007) Synaptic islands defined by the
763 territory of a single astrocyte. J Neurosci 27:6473-7. https://doi.org/10.1523/jneurosci.1419-07.2007
764 Harris KD, Shepherd GM (2015) The neocortical circuit: themes and variations. Nat Neurosci 18:170-
765 81. https://doi.org/10.1038/nn.3917
766 Hochstim C, Deneen B, Lukaszewicz A, Zhou Q, Anderson DJ (2008) Identification of positionally
767 distinct astrocyte subtypes whose identities are specified by a homeodomain code. Cell 133:510-22.
768 https://doi.org/10.1016/j.cell.2008.02.046
769 Johnson SJ, Walker FR (2015) Strategies to improve quantitative assessment of immunohistochemical
770 and immunofluorescent labelling. Sci Rep 5:10607. https://doi.org/10.1038/srep10607
771 Lago-Baldaia I, Fernandes VM, Ackerman SD (2020) More Than Mortar: Glia as Architects of
772 Nervous System Development and Disease. Front Cell Dev Biol 8:611269.
773 https://doi.org/10.3389/fcell.2020.611269

774 Lanjakornsiripan D, Pior BJ, Kawaguchi D, Furutachi S, Tahara T, Katsuyama Y, Suzuki Y, Fukazawa
775 Y, Gotoh Y (2018) Layer-specific morphological and molecular differences in neocortical astrocytes
776 and their dependence on neuronal layers. Nat Commun 9:1623. https://doi.org/10.1038/s41467-018-
777 03940-3
778 LaPlaca MC, Cullen DK, McLoughlin JJ, Cargill RS, 2nd (2005) High rate shear strain of three-
779 dimensional neural cell cultures: a new in vitro traumatic brain injury model. J Biomech 38:1093-105.
780 https://doi.org/10.1016/j.jbiomech.2004.05.032
781 Liu H, Caballero-Florán RN, Hergenreder T, Yang T, Hull JM, Pan G, Li R, Veling MW, Isom LL,
782 Kwan KY, Huang ZJ, Fuerst PG, Jenkins PM, Ye B (2023) DSCAM gene triplication causes excessive
783 GABAergic synapses in the neocortex in Down syndrome mouse models. PLoS Biol 21:e3002078.
784 https://doi.org/10.1371/journal.pbio.3002078
785 Long KR, Huttner WB (2019) How the extracellular matrix shapes neural development. Open Biol
786 9:180216. https://doi.org/10.1098/rsob.180216
787 Marchetti G, Escuin S, van der Flier A, De Arcangelis A, Hynes RO, Georges-Labouesse E (2010)
788 Integrin alpha5beta1 is necessary for regulation of radial migration of cortical neurons during mouse
789 brain development. Eur J Neurosci 31:399-409. https://doi.org/10.1111/j.1460-9568.2009.07072.x
790 Maynard KR, Stein E (2012) DSCAM contributes to dendrite arborization and spine formation in the
791 developing cerebral cortex. J Neurosci 32:16637-50. https://doi.org/10.1523/jneurosci.2811-12.2012
792 Mubuchi A, Takechi M, Nishio S, Matsuda T, Itoh Y, Sato C, Kitajima K, Kitagawa H, Miyata S
793 (2024) Assembly of neuron- and radial glial-cell-derived extracellular matrix molecules promotes
794 radial migration of developing cortical neurons. Elife 12:e92342. https://doi.org/10.7554/eLife.92342
795 Noble M, Fok-Seang J, Cohen J (1984) Glia are a unique substrate for the in vitro growth of central
796 nervous system neurons. J Neurosci 4:1892-903. https://doi.org/10.1523/jneurosci.04-07-01892.1984
797 Purohit AA, Li W, Qu C, Dwyer T, Shao Q, Guan KL, Liu G (2012) Down syndrome cell adhesion
798 molecule (DSCAM) associates with uncoordinated-5C (UNC5C) in netrin-1-mediated growth cone

799 collapse. J Biol Chem 287:27126-38. https://doi.org/10.1074/jbc.M112.340174
800 Rakic P (2007) The radial edifice of cortical architecture: from neuronal silhouettes to genetic
801 engineering. Brain Res Rev 55:204-19. https://doi.org/10.1016/j.brainresrev.2007.02.010
802 Satterstrom FK, Kosmicki JA, Wang J, Breen MS, De Rubeis S, An JY, Peng M, Collins R, Grove J,
803 Klei L, Stevens C, Reichert J, Mulhern MS, Artomov M, Gerges S, Sheppard B, Xu X, Bhaduri A,
804 Norman U, Brand H, Schwartz G, Nguyen R, Guerrero EE, Dias C, Betancur C, Cook EH, Gallagher
805 L, Gill M, Sutcliffe JS, Thurm A, Zwick ME, Børglum AD, State MW, Cicek AE, Talkowski ME,
806 Cutler DJ, Devlin B, Sanders SJ, Roeder K, Daly MJ, Buxbaum JD (2020) Large-Scale Exome
807 Sequencing Study Implicates Both Developmental and Functional Changes in the Neurobiology of
808 Autism. Cell 180:568-584.e23. https://doi.org/10.1016/j.cell.2019.12.036
809 Schindelin J, Arganda-Carreras I, Frise E, Kaynig V, Longair M, Pietzsch T, Preibisch S, Rueden C,
810 Saalfeld S, Schmid B, Tinevez JY, White DJ, Hartenstein V, Eliceiri K, Tomancak P, Cardona A
811 (2012) Fiji: an open-source platform for biological-image analysis. Nat Methods 9:676-82.
812 https://doi.org/10.1038/nmeth.2019
813 Schmucker D, Clemens JC, Shu H, Worby CA, Xiao J, Muda M, Dixon JE, Zipursky SL (2000)
814 Drosophila Dscam is an axon guidance receptor exhibiting extraordinary molecular diversity. Cell
815 101:671-84. https://doi.org/10.1016/s0092-8674(00)80878-8
816 Sekine K, Honda T, Kawauchi T, Kubo K, Nakajima K (2011) The outermost region of the developing
817 cortical plate is crucial for both the switch of the radial migration mode and the Dab1-dependent
818 "inside-out" lamination in the neocortex. J Neurosci 31:9426-39.
819 https://doi.org/10.1523/jneurosci.0650-11.2011
820 Sekine K, Kawauchi T, Kubo K, Honda T, Herz J, Hattori M, Kinashi T, Nakajima K (2012) Reelin
821 controls neuronal positioning by promoting cell-matrix adhesion via inside-out activation of integrin
822 α5β1. Neuron 76:353-69. https://doi.org/10.1016/j.neuron.2012.07.020
823 Sofroniew MV, Vinters HV (2010) Astrocytes: biology and pathology. Acta Neuropathol 119:7-35.

824 https://doi.org/10.1007/s00401-009-0619-8
825 Takahashi T, Goto T, Miyama S, Nowakowski RS, Caviness VS, Jr. (1999) Sequence of neuron origin
826 and neocortical laminar fate: relation to cell cycle of origin in the developing murine cerebral wall. J
827 Neurosci 19:10357-71. https://doi.org/10.1523/jneurosci.19-23-10357.1999
828 Takeuchi M, Yamaguchi S, Yonemura S, Kakiguchi K, Sato Y, Higashiyama T, Shimizu T, Hibi M
829 (2015) Type IV Collagen Controls the Axogenesis of Cerebellar Granule Cells by Regulating
830 Basement Membrane Integrity in Zebrafish. PLoS Genet 11:e1005587.
831 https://doi.org/10.1371/journal.pgen.1005587
832 Tang XY, Xu L, Wang J, Hong Y, Wang Y, Zhu Q, Wang D, Zhang XY, Liu CY, Fang KH, Han X,
833 Wang S, Wang X, Xu M, Bhattacharyya A, Guo X, Lin M, Liu Y (2021) DSCAM/PAK1 pathway
834 suppression reverses neurogenesis deficits in iPSC-derived cerebral organoids from patients with
835 Down syndrome. J Clin Invest 131:e135763. https://doi.org/10.1172/jci135763
836 Thiry L, Lemieux M, Bretzner F (2018) Age- and speed-dependent modulation of gaits in DSCAM(2J)
837 mutant mice. J Neurophysiol 119:723-737. https://doi.org/10.1152/jn.00471.2017
838 Thomsen MS, Routhe LJ, Moos T (2017) The vascular basement membrane in the healthy and
839 pathological brain. J Cereb Blood Flow Metab 37:3300-3317.
840 https://doi.org/10.1177/0271678x17722436
841 Tiklová K, Björklund Å K, Lahti L, Fiorenzano A, Nolbrant S, Gillberg L, Volakakis N, Yokota C,
842 Hilscher MM, Hauling T, Holmström F, Joodmardi E, Nilsson M, Parmar M, Perlmann T (2019)
843 Single-cell RNA sequencing reveals midbrain dopamine neuron diversity emerging during mouse
844 brain development. Nat Commun 10:581. https://doi.org/10.1038/s41467-019-08453-1
845 Tsai HH, Li H, Fuentealba LC, Molofsky AV, Taveira-Marques R, Zhuang H, Tenney A, Murnen AT,
846 Fancy SP, Merkle F, Kessaris N, Alvarez-Buylla A, Richardson WD, Rowitch DH (2012) Regional
847 astrocyte allocation regulates CNS synaptogenesis and repair. Science 337:358-62.
848 https://doi.org/10.1126/science.1222381

Xu L, Nirwane A, Yao Y (2019) Basement membrane and blood-brain barrier. Stroke Vasc Neurol 4:78-82. https://doi.org/10.1136/svn-2018-000198

Xu Y, Ye H, Shen Y, Xu Q, Zhu L, Liu J, Wu JY (2011) Dscam mutation leads to hydrocephalus and decreased motor function. Protein Cell 2:647-55. https://doi.org/10.1007/s13238-011-1072-8

Yamagata M, Sanes JR (2008) Dscam and Sidekick proteins direct lamina-specific synaptic connections in vertebrate retina. Nature 451:465-9. https://doi.org/10.1038/nature06469

Yamakawa K, Huot YK, Haendelt MA, Hubert R, Chen XN, Lyons GE, Korenberg JR (1998) DSCAM: a novel member of the immunoglobulin superfamily maps in a Down syndrome region and is involved in the development of the nervous system. Hum Mol Genet 7:227-37. https://doi.org/10.1093/hmg/7.2.227

Zagaglia S, Selch C, Nisevic JR, Mei D, Michalak Z, Hernandez-Hernandez L, Krithika S, Vezyroglou K, Varadkar SM, Pepler A, Biskup S, Leão M, Gärtner J, Merkenschlager A, Jaksch M, Møller RS, Gardella E, Kristiansen BS, Hansen LK, Vari MS, Helbig KL, Desai S, Smith-Hicks CL, Hino-Fukuyo N, Talvik T, Laugesaar R, Ilves P, Õunap K, Körber I, Hartlieb T, Kudernatsch M, Winkler P, Schimmel M, Hasse A, Knuf M, Heinemeyer J, Makowski C, Ghedia S, Subramanian GM, Striano P, Thomas RH, Micallef C, Thom M, Werring DJ, Kluger GJ, Cross JH, Guerrini R, Balestrini S, Sisodiya SM (2018) Neurologic phenotypes associated with COL4A1/2 mutations: Expanding the spectrum of disease. Neurology 91:e2078-e2088. https://doi.org/10.1212/wnl.0000000000006567

Zhou Y, Zhou B, Pache L, Chang M, Khodabakhshi AH, Tanaseichuk O, Benner C, Chanda SK (2019) Metascape provides a biologist-oriented resource for the analysis of systems-level datasets. Nat Commun 10:1523. https://doi.org/10.1038/s41467-019-09234-6

Statements and Declarations

Ethics approval and consent to participate

All animal experiments were conducted in accordance with the Tohoku University Guidelines for Animal Experimentation and were approved by the Institutional Animal Care and Use Committee of Tohoku University (Approval No. 2024PhA-005).

Consent for publication

Not applicable.

Availability of data and materials

The mass spectrometry proteomics data are being deposited to the ProteomeXchange Consortium via the PRIDE partner repository. The dataset accession number will be provided upon completion of the submission process. Supplementary information is available with the online version of this article.

Competing interests

The authors declare that they have no competing interests.

Funding

This work was supported by the Japan Agency for Medical Research and Development (AMED) under grant number JP24wm0625508 (N.A.), Japan Society for the Promotion of Science KAKENHI Grant-in-Aid for Scientific Research (B) under grant number 24K01943 (N.A.), Japan Science and Technology Agency under grant number JPMJCR21P1 and JPMJMS2292 (T.S.) and research grants from the Astellas Foundation for Research on Metabolic Disorders, the Sumitomo Foundation, and the Daiichi Sankyo Foundation of Life Science.

Authors' contributions

K.H., T.S. and N.A. supervised the study. K.H., T.I., T.N., and N.A. performed the experiments. K.H., T.I., T.N. and N.A. contributed to data analysis. K.H. and N.A. wrote the manuscript. K.H., T.I., T.N., T.S. and N.A. discussed the results and commented on the manuscript. All authors read and approved the final manuscript.

Declaration of Generative AI and AI-assisted technologies in the writing process

During the preparation of this manuscript, the authors used ChatGPT (OpenAI) to improve the grammar, language, and readability of the manuscript. The authors reviewed and edited the AI-assisted suggestions and take full responsibility for the final content of the manuscript.

Supplementary Information

Online Resource 1 Supplementary Table 1. ASOs used in this study. Sequences and chemical modifications of the control, Dscam-targeting, and Col4a2-targeting antisense oligonucleotides.

Online Resource 2 Supplementary Table 2. Candidate DSCAM-associated proteins identified by LC–MS/MS analysis of E15 *Dscam*-3×ALFA knock-in mouse brains. Unnormalized protein intensity values are provided.

Supplementary Files

This is a list of supplementary files associated with this preprint. Click to download.

- OnlineResource1Hizawa.pdf
- OnlineResource2Hizawa.xlsx